Title

Canine peripheral blood TCRαβ T cell atlas: Identification of diverse subsets including CD8A+ MAIT-like cells by combined single-cell transcriptome and V(D)J repertoire analysis

Authors

Eschke, Maria
Moore, Peter F
Chang, Haiyang
et al.

Publication Date

2023

DOI

10.3389/fimmu.2023.1123366

Peer reviewed

frontiers | Frontiers in Immunology

TYPE Original Research
PUBLISHED 23 February 2023
DOI 10.3389/fimmu.2023.1123366

OPEN ACCESS

EDITED BY
Robert David Miller,
University of New Mexico, United States

REVIEWED BY
Kerstin Mair,
University of Veterinary Medicine Vienna, Austria
Stephanie Christina Talker,
University of Bern, Switzerland

*CORRESPONDENCE
Maria Eschke
maria.eschke@bbz.uni-leipzig.de

SPECIALTY SECTION
This article was submitted to Comparative Immunology, a section of the journal Frontiers in Immunology

RECEIVED 13 December 2022
ACCEPTED 19 January 2023
PUBLISHED 23 February 2023

CITATION
Eschke M, Moore PF, Chang H, Alber G and Keller SM (2023) Canine peripheral blood TCRαβ T cell atlas: Identification of diverse subsets including CD8A$^+$ MAIT-like cells by combined single-cell transcriptome and V(D)J repertoire analysis.
Front. Immunol. 14:1123366.
doi: 10.3389/fimmu.2023.1123366

Canine peripheral blood TCRαβ T cell atlas: Identification of diverse subsets including CD8A$^+$ MAIT-like cells by combined single-cell transcriptome and V(D)J repertoire analysis

Maria Eschke[1]*, Peter F. Moore[2], Haiyang Chang[3], Gottfried Alber[1] and Stefan M. Keller[2]

[1]Institute of Immunology/Molecular Pathogenesis, Center for Biotechnology and Biomedicine, College of Veterinary Medicine, University of Leipzig, Leipzig, Germany, [2]Department of Pathology, Microbiology and Immunology, School of Veterinary Medicine, University of California, Davis, CA, United States, [3]Department of Mathematics and Statistics, University of Guelph, Guelph, ON, Canada

The dog is valued as a companion animal and increasingly recognized as a model for human disorders. Given the importance of T cells in health and disease, comprehensive knowledge of canine T cells can contribute to our understanding of pathogenesis mechanisms and inform the development of new treatment strategies. However, the diversity of canine T cells is still poorly understood mainly due to the lack of species-reactive antibodies for use in flow cytometry. The aim of this study was to generate a detailed atlas of peripheral blood TCRαβ$^+$ T cells of healthy dogs using single-cell RNA-sequencing (scRNAseq) combined with immune repertoire sequencing. A total of 22 TCRαβ$^+$ T cell clusters were identified, which were classified into three major groups: CD4-dominant (11 clusters), CD8A-dominant (8 clusters), and CD4/CD8A-mixed (3 clusters). Based on differential gene expression, distinct differentiation states (naïve, effector, memory, exhausted) and lineages (e.g. CD4 T helper and regulatory T cells) could be distinguished. Importantly, several T cell populations were identified, which have not been described in dogs before. Of particular note, our data provide first evidence for the existence of canine mucosa-associated invariant T cell (MAIT)-like cells, representing one of three newly identified FCER1G$^+$ innate-like CD8A$^+$ T cell populations in the peripheral blood of healthy dogs. In conclusion, using scRNAseq combined with immune repertoire sequencing we were able to resolve canine TCRαβ$^+$ T cell populations at unprecedented resolution. The peripheral blood TCRαβ$^+$ T cell atlas of healthy dogs generated here represents an important reference data set for future studies and is of relevance for identifying new targets for T cell-specific therapies.

KEYWORDS

dog, canine T cells, TCRαβ, single-cell RNA-sequencing, immune repertoire, peripheral blood, MAIT-like cells, innate-like T cells

1 Introduction

An in-depth understanding of the physiological and pathophysiological processes in different species is of increasing importance in the fields of vaccinology and immunotherapy. Considering interspecies differences of immune cells, it is essential to unveil species-specific characteristics. Several features of dogs (*Canis lupus familiaris*) make this species an attractive candidate for immunotherapy research. As companion animals, dogs are largely exposed to the same environmental conditions as humans and develop common human health disorders, including autoimmune diseases (1), allergies (2), and cancer (3). T lymphocytes expressing the T cell receptor (TCR) αβ are well-known to play a central role in adaptive immunity across species and are therefore promising targets for immunotherapies. However, the diversity of canine TCRαβ$^+$ T cells is still incompletely understood, primarily due to the paucity of dog-reactive immunophenotyping reagents for use in flow cytometry as well as insufficient *a priori* knowledge of marker genes. Single-cell RNA-sequencing (scRNA-seq) enables unbiased, high throughput and high-resolution transcriptomic analysis of heterogeneous cell populations with a multitude of applications across biomedical sciences (4). In non-traditional model organisms, scRNA-seq has been shown to present a powerful tool to characterize the cellular diversity of immune cells (5–7).

In the canine species, scRNA-seq has been used previously to identify cellular populations of the bronchoalveolar lavage fluid of healthy dogs (6) and to evaluate the expression patterns of SARS-CoV-2 entry factors in lung cells (8). However, both studies neither resolved CD4$^+$ and CD8$^+$ T cell subpopulations nor analysed the immune repertoire.

Here, we used the potential of scRNA-seq in combination with immune repertoire sequencing to generate a highly detailed atlas of peripheral blood TCRαβ$^+$ T cells of healthy dogs. A total of 22 TCRαβ$^+$ T cell clusters were identified and divided into three major groups: (i) a CD4-dominant group containing 11 clusters, (ii) a CD8A-dominant group containing eight clusters, and (iii) a CD4/CD8A-mixed group containing three clusters. Besides well-known CD4 and CD8A T cell differentiation states (naïve, effector, memory) and lineages (e.g. T helper and regulatory CD4 T cells), our comprehensive analysis revealed several novel T cell subtypes not previously identified in dogs, including a MAIT-like population characterized by a highly restricted TCR repertoire. The combined transcriptome and V(D)J immune-repertoire analysis provided important reference data highlighting the cellular heterogeneity of peripheral blood TCRαβ$^+$ T cells of healthy dogs. It can be referenced in future experiments to elucidate tissue-specific properties of the individual T cell populations under both physiological and pathophysiological conditions.

2 Materials and methods

2.1 Dogs, blood sample collection

From 4 healthy experimental Beagle dogs (Table 1, one female, three male, age: 5 – 9 years) of the Faculty of Veterinary Medicine (Leipzig University, Leipzig, Germany), venous blood was taken by venipuncture of the *vena cephalica antebrachii* into heparinized vacutainer tubes (BD Vacutainer®, 10 ml, Li-Heparin 17 IU/ml Becton Dickinson, Heidelberg, Germany). All dogs received routine vaccinations against canine distemper, rabies, canine infectious hepatitis, parvovirus infection, parainfluenza, and leptospirosis. The study was authorized by the Saxony State Office (*Landesdirektion Sachsen*) in Leipzig, Germany (approval number: DD24.1-5131/444/30).

2.2 Isolation of canine peripheral blood mononuclear cells

PBMC were isolated by density gradient centrifugation. Briefly, blood was diluted at a ratio of 1:1 with phosphate buffered saline (PBS), layered above Biocoll Separating Solution (density 1077 g/l, Biochrom AG, Berlin, Germany) and centrifuged at 500 x g for 30 min at room temperature (RT) without brake. PBMC at the interphase were harvested into PBS and centrifuged at 500 x g for 10 min at RT. After another washing step with PBS, erythrocytes were lysed by incubation in 150 mM NH_4Cl, 8 mM $KHCO_3$, 2 mM EDTA (pH 7) for 5 min at RT. The reaction was stopped by addition of PBS containing 3% fetal bovine serum (FBS, Thermo Fisher Scientific, Carlsbad, USA; and PAN-Biotech, Aidenbach, Germany). After washing with PBS, PBMC were counted in Trypan blue (Sigma-Aldrich, Taufkirchen, Germany) using a hemocytometer (Laboroptik, Lancing, UK).

2.3 Fluorescence-activated cell sorting of TCRαβ$^+$ T cells

PBMC were first stained with the fixable viability dye eFluor 780 (Thermo Fisher Scientific, Carlsbad, USA) according to the

TABLE 1 Subject characteristics as well as sequencing and mapping quality control metrics for each dog.

Study subject	Sex	Age (years)	Estimated number of cells	Reads mapped confidently to:		Median genes per cell	Median UMI counts per cell	Total genes detected
				Genome	Transcriptome			
DOG 1	F	5	7,428	72.3%	41.0%	1,394	3,534	13,649
DOG 2	M	7	8,873	73.2%	42.3%	1,534	3,844	13,849
DOG 3	M	7	8,402	72.5%	41.2%	1,498	3,716	13,720
DOG 4	M	9	8,422	73.3%	42.1%	1,561	3,809	13,667

manufacturer's protocol to discriminate dead from viable cells. In a second step, they were incubated with a mixture of heat-inactivated normal serum derived from dog and rat (each 15% in PBS) to block unspecific binding of Fc receptors. Then, cells were incubated with anti-canine TCRαβ (clone CA15.8G7) hybridoma supernatant, for 15 min in the dark on ice. A PerCP/Cy5.5-conjugated goat-anti-mouse IgG secondary antibody (Biolegend, San Diego, USA) was used for detection. Sorting was performed using the BD FACSAria™ III flow cytometer (Becton Dickinson, Heidelberg, Germany). The sorting strategy is shown in Figure 1B. After exclusion of dead cells and doublets, TCRαβ$^+$ T cells from the lymphocyte gate were sorted with a purity >99% (Re-analysis using the FlowJo™10 software (Treestar Inc., Ashland, OR, USA). Isolated TCRαβ$^+$ T cells were cryopreserved in 90% FBS, 10% dimethyl sulfoxide (Sigma-Aldrich) and shipped on dry ice to the Institute of Pathology, Microbiology & Immunology of the UC Davis.

2.4 Single-cell 5' RNA and V(D)J sequencing

All 4 samples were thawed at once so that scRNA-Seq could be performed in a single run to avoid batch-specific effects. After confirmation of cellularity (1.1-1.4 x 10^6 cells/ml) and viability (78-90%) of TCRαβ$^+$ T cells, transcriptome and V(D)J libraries were prepared at the UC Davis Genome Center. Briefly, ~10,000 TCRαβ$^+$ T cells per lane were loaded on a Chromium Single Cell Controller (10× Genomics, Pleasanton, CA, USA). Within individual gel beads in emulsion (GEMs), captured cells were lysed and the released RNAs were barcoded through reverse transcription. Starting mRNA molecules were indexed using Unique Molecular Identifier (UMI). Following emulsion breakage, barcoded cDNA was amplified and libraries were constructed using the Chromium Next GEM Single Cell 5' Kit v2 (10x Genomics). The canine T cell receptor alpha (TRA) and T cell receptor beta (TRB) genes were amplified using the Chromium Single Cell V(D)J Enrichment Kit according to the manufacturer's instructions but with primers adapted for the canine genes (see Supplementary Table 1 for primer sequences and additional information). Libraries were sequenced using the Illumina NovaSeq S4 platform using 150 paired-end reads to a target read depth of 30,000 reads per cell. Single-cell data were pre-processed using the Cell Ranger software 5.0.1 (10x Genomics). The standard workflow was used for alignment of reads to the reference genome (CanFam 3.1 annotation genebuild updated 2019-06, GenBank assembly accession: GCA_000002285). Reads were organized by cell barcodes and UMI counting resulting in a digital expression (gene-cell barcode) matrix. scRNA-seq data are available in the NCBI GEO repository, accession number GSE218355.

2.5 Transcriptome data analysis

The digital gene expression matrix resulting from data preprocessing was analyzed using the R package Seurat v4.1.1 (9, 10). Analysis R code is available upon request. Briefly, genes expressed in fewer than three cells per subject were excluded. Data from all four dogs were merged, and cells with less than 500 or more than 20,000 UMIs (transcripts) as well as low quality/dying cells with greater than 10% UMIs assigned to mitochondrial genes were excluded. Following filtering, the global-scaling normalization method "LogNormalize" was applied, and variable genes were set to all genes after filtering.

Principal component analysis (PCA) was used for dimensionality reduction and unsupervised graph-based clustering (resolution factor 1.61) was performed on the first 50 principal components. Different resolution factors were tested and cluster stability was evaluated using the clustree package (11). Additional subdivisions of clusters at higher resolutions were not associated with further detection of informative differentially expressed genes. The data were visualized by non-linear dimensional reduction using uniform manifold approximation and projection (UMAP) plots. The FindAllMarkers function was used to identify differentially expressed genes (DEGs) across clusters

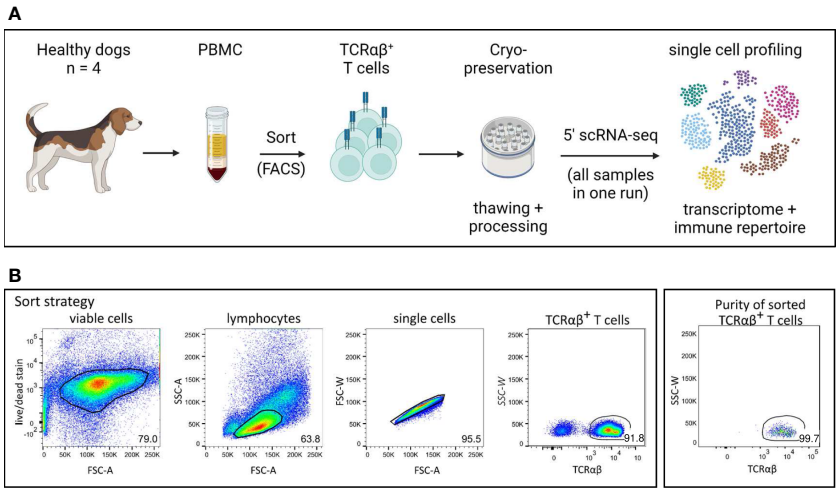

FIGURE 1
Experimental setup for single cell analysis of canine TCRαβ$^+$ T cells. **(A)** Peripheral blood mononuclear cells (PBMC) of four healthy Beagle dogs were used. Cryopreserved TCRαβ$^+$ T cells isolated by fluorescence-activated cell sorting (FACS) were applied to 5' single-cell RNA sequencing (5' scRNA-seq) for integrated transcriptome and TCR repertoire analysis. (created with BioRender) **(B)** The gating strategy for isolation of TCRαβ$^+$ T cells by FACS as well as the purity of the sorted population are shown (representative data of one dog). Numbers in plots imply percentages.

(Supplementary Table 2). Some DEGs not annotated in the reference genome were further blasted on the Ensembl genome browser v108) (12) for dog species to increase the annotation rate. Cell clusters were manually annotated based on expression of T cell signature genes, primarily known from human and mouse studies. ViolinPlots, DotPlots, and FeaturePlots were used for visualizing differences in gene expression between clusters.

2.6 V(D)J data analysis

All basic analyses were done using the R software (version 4.1.2) and the following packages: circlize (chord diagrams), ggseqlogo (sequence logos), igraph (centrality), RColorBrewer (colors), stringdist (Hamming distance), tidy code (tidyverse). To identify clusters in the TRA and TRB datasets, junctional amino acid sequences were first stratified by V and J gene subgroups followed by hierarchical clustering using the single and complete linkage methods and a cut-off of one Hamming Distance (HD). This resulted in clusters comprising one or multiple clonotypes. All clusters were numbered, regardless of how many clonotypes they contained. Pairwise amino acid comparison and hierarchical clustering were done using the Python software (version 3.10.2).

2.7 Statistical analysis

Differential gene expression was measured using non-parametric Wilcoxon rank sum tests adjusted for multiple testing with Bonferroni correction. Only significant DEGs with an adjusted *P*-value < 0.05 were retained.

3 Results

3.1 Single-cell RNA-sequencing of canine TCRαβ$^+$ T cells resolves CD8A-dominant, CD4-dominant, and CD4/CD8A-mixed clusters

In this study, we used combined transcriptome and V(D)J analysis at the single cell level to establish a detailed baseline TCRαβ$^+$ T cell atlas of the dog. Cryopreserved viable TCRαβ$^+$ T cells isolated with high purity (>99%) from peripheral blood of four healthy Beagle dogs by fluorescence-activated cell sorting (FACS) were applied to 5' single-cell RNA sequencing analysis (5' scRNA-seq) (Figure 1). Sequencing and mapping quality control metrics for each dog are summarized in Table 1. Unsupervised clustering of 31,909 cells from four dogs was performed for different resolution levels and a final resolution with 22 clusters was chosen. (Figure 2A). All clusters were present in each individual dog (Supplementary Figure 1). Violin plots visualizing CD8A and CD4 expression indicated the presence of CD8A$^+$, CD4$^+$ and CD8A$^+$/CD4$^+$ mixed clusters (Figure 2B). However, especially clusters in which CD4 was detected also contained a considerable proportion of cells without CD4 expression (Figure 2B), a phenomenon already observed in previous scRNA-seq studies using equine or human PBMC (5, 13). The number of TCRαβ$^+$ CD8α$^-$CD4$^-$ double-negative (dn) T cells detected by scRNA-seq was higher than what would be expected based on previous flow cytometric analyses [~15% (14)]. To better characterize the proportion of CD8A/CD4 expression in each cluster, CD8A$^-$CD4$^-$ dn cells were excluded and the percentage of CD8A$^+$ single-positive (sp) cells, CD4$^+$ sp cells, and CD4$^+$CD8A$^+$ double-positive (dp) cells of each cluster was evaluated (Figure 2C). Eight clusters consisting mainly of CD8A sp T cells were detected (C7, C12-C14, C16-C19). The proportion of CD8A$^+$ sp cells within those clusters was 95-99% except for clusters 14 and 16 (~80% CD8A$^+$ sp), which also contained CD4 sp (C16: ~12%) and/or CD4$^+$CD8A$^+$ dp T cells (C14: 18%, C16: 7%). Therefore, clusters C7, C12-C14, and C16-C19 were classified as CD8A-dominant. Besides clear-cut CD4 clusters with 89-98% of the cells showing a CD4 sp phenotype (C0-C3, C9, C10), several clusters showed dominance of CD4$^+$ sp cells but additionally comprised >10% CD8A$^+$ sp and/or CD4$^+$CD8A$^+$ dp T cells. Of those, clusters consisting of ≥66% CD4 sp T cells and <25% CD8A$^+$ sp cells were classified as CD4-dominant (C4-C6, C8, C15). The remaining three clusters (C11, C20-C21) with 35-41% CD8A$^+$ sp cells and 56-63% CD4$^+$ sp cells were classified as CD4/CD8A-mixed. Notably, only a small proportion (1-6%) of cells within the latter group had a CD4$^+$CD8A$^+$ dp phenotype (Figure 2C).

Taken together, based on the proportions of CD8A$^+$ and CD4$^+$ cells, clusters were divided into three major groups: (i) a CD4-dominant group containing eleven clusters (C0-C6, C8-C10, C15), (ii) a CD8A-dominant group containing eight clusters (C7, C12-C14, C16-C19), and (iii) a CD4/CD8A-mixed group containing three clusters (C11, C20, C21) (Figure 2C).

3.2 CD4-dominant clusters contain known T helper/T regulatory subsets as well as subsets previously unrecognized in dogs

Clusters of the three major groups of TCRαβ T cells were manually annotated by assessing the expression of lineage-defining marker genes. Two naïve TCRαβ$^+$ CD4 T cell clusters (C2, C3) were identified based on elevated expression of the lymph node homing receptors CCR7 and SELL (encoding CD62L/L-Selectin) as well as of the transcription factors TCF7 and LEF1 (13) (Figure 3A). As expected, the frequency of naïve CD4 T cells was lowest in the oldest and highest in the youngest dog (Table 2 and Supplementary Figure 1).

A direct comparison between the two clusters containing naïve CD4$^+$ T cells revealed that C2 expressed higher levels of quiescence-associated genes HOMER2, CCR7, SELL, KLF3, and IL7R (15–18) compared to C3 (Supplementary Figure 2 and Supplementary Table 3). Among the genes with higher expression in C3 compared to C2 were genes encoding interferon-induced transmembrane proteins (IFITM) and metallothionin (MT) (Supplementary Figure 2 and Supplementary Table 3). IFITM proteins as well as MT have been shown to be involved in differentiation of naive CD4 T cells (19, 20). Whereas C2 is more abundant than C3 in dogs 2, 3, and 4, the opposite was true for the youngest dog (dog 1) (Table 2 and Supplementary Figure 1).

C0, which was similarly abundant in all dogs (Table 2 and Supplementary Figure 1), was identified as resting central memory CD4 T cell cluster based on elevated expression of CCR7, TCF7 and SAMHD1 (13, 21–23) (Figure 3A). C4 was characterized by increased

10.3389/fimmu.2023.1123366

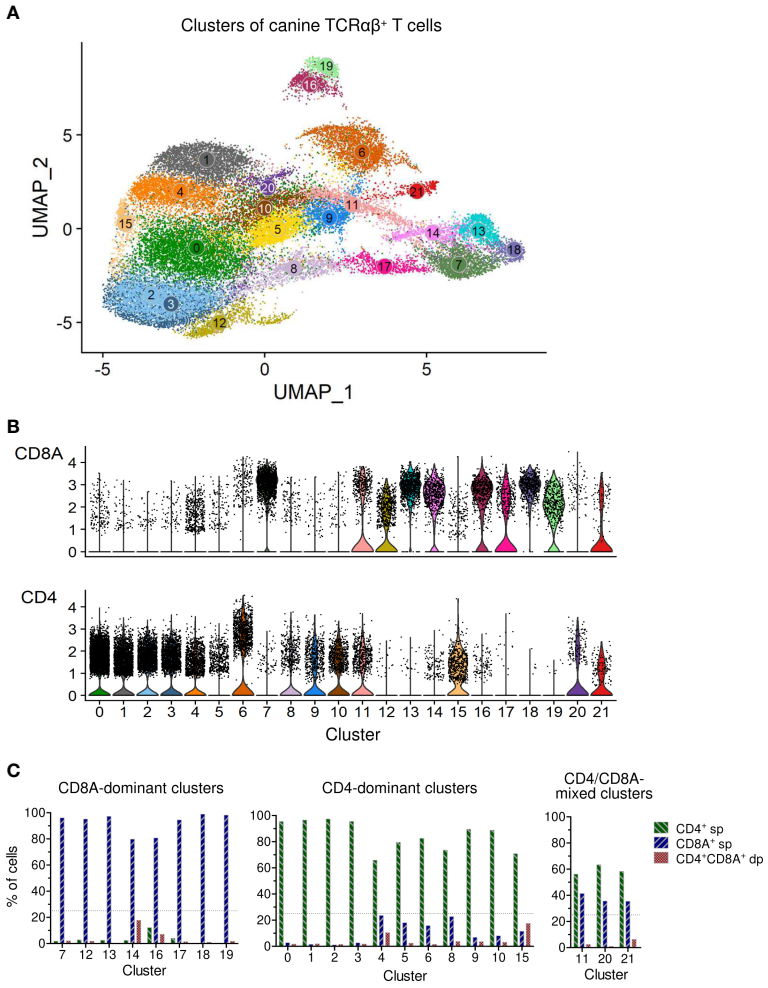

FIGURE 2
Single-cell RNA-sequencing analysis of TCRαβ$^+$ T cells purified from peripheral blood of healthy dogs revealed various CD8A-dominant, CD4-dominant and CD4/CD8A-mixed clusters. **(A)** Unsupervised graph-based clustering of merged data from all four dogs yielded 22 Clusters of canine TCRαβ$^+$ T cells. **(B)** Visualization of CD8A and CD4 expression by violin plots. **(C)** The percentage of CD8A$^+$ single-positive (sp), CD4$^+$ sp and CD4$^+$CD8A$^+$ double-positive (dp) T cells of each cluster was determined by virtual gating after exclusion of CD4$^-$CD8A$^-$ double-negative cells. Based on the CD8A/CD4 expression pattern, clusters were devided into three major groups: (1) CD8A-dominant (n = 8: C7, C12-14, C16-19), (2) CD4-dominant (n=11: C0-C6, C8-C10, C15), and (3) CD4/CD8A-mixed clusters (n = 3: C11, C20-21), mainly composed of CD8A$^+$ and CD4$^+$ sp cells. Dotted line: treshold for maximum CD4$^+$/CD8A$^+$ sp cells in CD8A/CD4-dominant clusters.

expression of the killer cell lectin-like receptor K1 (KLRK1) encoding NKG2D, a prototypical activation marker on human and mouse NK cells mediating cytotoxicity (24, 25). Cytotoxic potential of cells within C4 was further supported by expression of the cytotoxic effector molecule granzyme K (GZMK), which was evident when C4 was compared against all other CD4-dominant clusters (Figure 3B and Supplementary Table 4). However, albeit classified as a CD4-dominant cluster, C4 also comprised CD8A$^+$ sp cells and CD4$^+$CD8A$^+$ dp cells (Figure 2C). To verify that CD4$^+$ sp cells in C4 contributed to the cytotoxic signature in this cluster, after exclusion of CD4$^-$CD8$^-$ dn cells, CD4$^+$ sp, CD8A$^+$ sp and CD4$^+$CD8A$^+$ dp cells were analyzed for expression of GZMK and KLRK1 separately. Indeed, cytotoxicity-associated genes were detected in all three fractions (Figure 3C) supporting the notion that cytotoxic CD4$^+$ T cells exist in dogs. Cytotoxic CD4$^+$ T cells are well described in mice and humans in the context of viral infections, autoimmunity, and cancer (26, 27). In humans, NKG2D$^+$ highly activated cytotoxic CD4$^+$ T cells have been associated with immune senescence (26, 28, 29). Although the low number of dogs used does not allow definite conclusions, an association of canine cytotoxic CD4$^+$ T cells with age was not supported by this study, as dog 1 (youngest) and dog 4 (oldest) had a lower frequency of cytotoxic CD4$^+$ T cells than dogs 2 and 3 (Table 2 and Supplementary Figure 1).

Distinct populations of CD4$^+$ T helper (Th) cells were resolved by scRNA-seq in this study. In C1, elevated expression of genes associated with the Th1 phenotype was detected, including IL18R1, CXCR3, IL12RB, and ALDOC (30–34). Although the master transcription factor of Th1 cells T-bet (encoded by TBX21) did not appear as DEG in C1, there was a trend of weak TBX21 expression among CD4-dominant clusters in C1 and C4 matching the Th1/cytotoxic CD4 phenotype (Figure 3B). Of note, low levels of TBX21 transcripts in canine CD4$^+$ T cells is consistent with our flow cytometric data suggesting IFN-γ production despite weak T-bet expression (35). Indeed, constitutive expression of IFNG encoding the Th1-effector cytokine was detected in C1. Noteworthy, CCR9, which, in addition to its role as gut homing molecule, has been shown

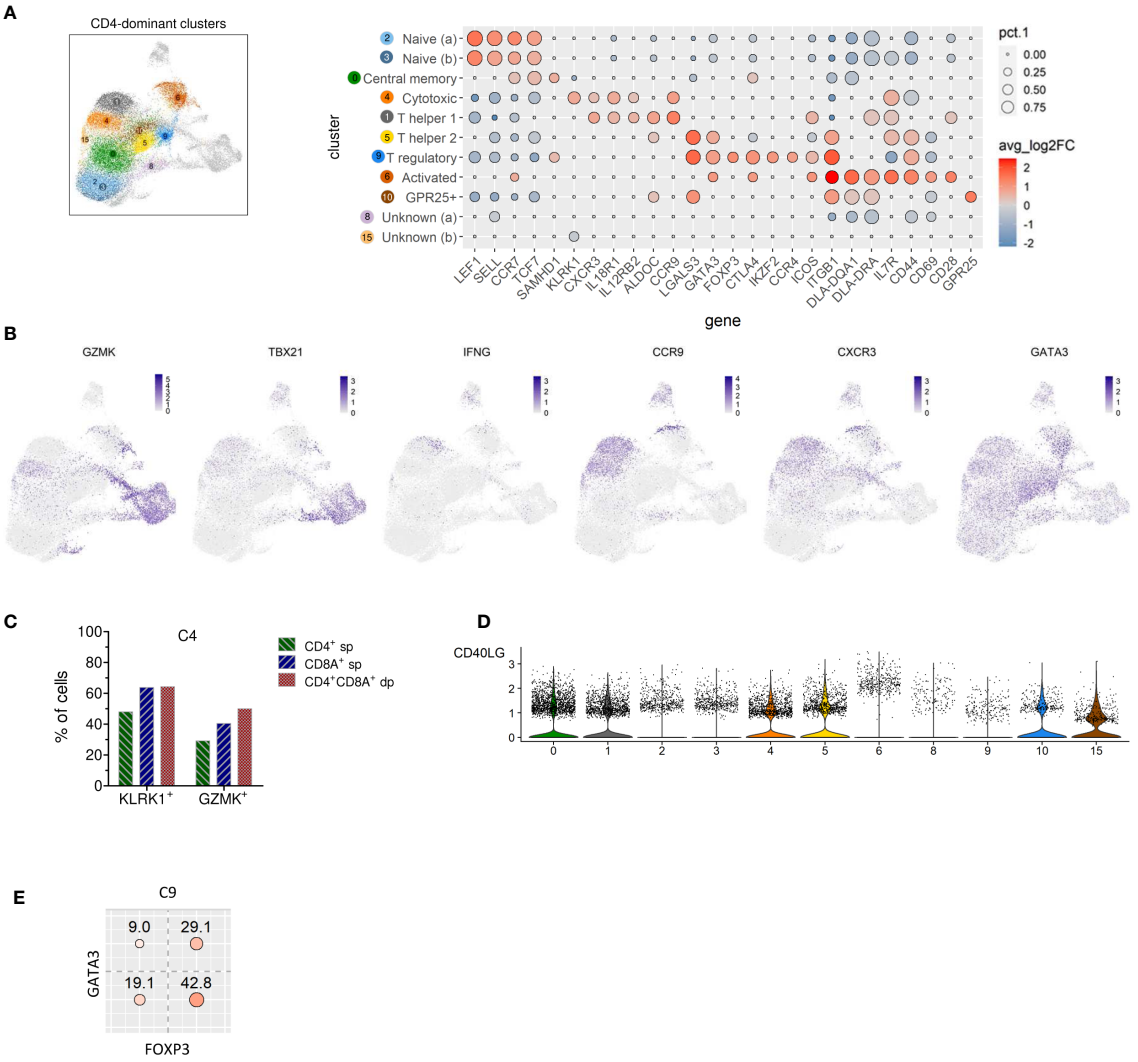

FIGURE 3
Identification of naive, memory and known T helper and regulatory subsets among canine TCRαβ$^+$ CD4-dominant clusters and detection of CD4 T cells with cytotoxic potential. **(A)** CD4 cell-dominat clusters highlighted in UMAP plot were annotated based on expression of T cell subset marker genes shown in Dot plot. The dot size corresponds to the percentage (pct.1) of cells expressing the gene in each CD4-dominant cluster, the color represents the expression level (average log2 fold change). Genes were ordered to visualize the differences/similarities between cell types. **(B)** Expression pattern of select genes across all canine TCRαβ$^+$ clusters visualized by FeaturePlots **(C)** Within C4, expression of the cytotoxic effector molecules KLRK1 and GZMK was detected in the dominating CD4$^+$ sp cells and in the minor fractions of CD8A$^+$ sp and CD4$^+$CD8A$^+$ dp T cells by virtual gating after exclusion of CD4$^-$CD8A$^-$ double-negative cells. **(D)** Visualization of CD40LG expression in CD4-dominant clusters by violin plots. **(E)** Virtual gating for FOXP3 and GATA3 within C9 (T regulatory CD4-dominant cluster) reveals co-expression of the transcription factors in ~30% of the cells.

to shape immune responses by inhibiting development of regulatory T (Treg) cells (36) appeared as top DEG of the CD4-dominant clusters C1 (Th1) and C4 (cytotoxic CD4$^+$ T cells) (Figure 3B). Individual differences were observed with respect to the proportions of these two clusters: In dog 1 (youngest), they only comprised few cells. Dog 4 (oldest) contained a large Th1 (C1) and rather small cytotoxic CD4$^+$ (C4) cluster, whereas the opposite was found for dog 2. In dog 3 both clusters represented large populations (Table 2 and Supplementary Figure 1).

C9 was identified as distinct Treg cluster expressing the marker genes FOXP3, CTLA4, IKZF2, and CCR4 (Figure 3A). Interestingly, FoxP3 and GATA3 were co-expressed in ~30% of cells in C9 (Figure 3E), confirming our previous flow cytometry results showing co-expression of both transcription factors in small fractions of canine CD4$^+$ T cells and CD4$^-$CD8A$^-$ dn T cells (14). In mice, co-expression of GATA-3 has been shown to stabilize FoxP3 expression and to prevent conversion of CD4$^+$ FoxP3$^+$ T cells into a pro-inflammatory Th17 cell phenotype (37–39).

Based on elevated GATA3 expression but lack of FoxP3, C5 was annotated as Th2 cell cluster (Figure 3A). Both, clusters 5 and 9 are characterized by expression of Galectin-3 (encoded by LGALS3). A Th2-promoting activity of Galectin-3 as well as its expression on Treg cells have been shown previously (40).

Interestingly, increased expression of LGALS3 was also found in a third cluster (C10). C10 is characterized by expression of GPR25, which encodes an orphan G protein-coupled receptor. CD4$^+$ GPR25$^+$ cells represent another previously unrecognized canine TCRαβ$^+$ T cell population.

Cluster 6 comprises activated TCRαβ$^+$ CD4$^+$ T cells defined by high expression of the early activation marker CD69 as well as of

10.3389/fimmu.2023.1123366

TABLE 2 Total number of cells of each TCRαβ$^+$ T cell cluster and their distribution among dogs.

Cluster	Total	DOG1	DOG2	DOG3	DOG4
C0: CD4 Central memory	4930	28.0%	25.6%	20.8%	25.7%
C1: CD4 T helper 1	2860	5.5%	9.6%	32.2%	52.7%
C2: CD4 Naive (a)	2849	16.7%	31.1%	43.1%	9.1%
C3: CD4 Naive (b)	2637	81.3%	6.4%	10.5%	1.8%
C4: CD4 Cytotoxic	2498	6.4%	43.8%	35.9%	13.9%
C5: CD4 T helper 2	2187	18.9%	27.9%	22.3%	30.9%
C6: CD4 Activated	2129	20.5%	12.7%	34.8%	31.9%
C7: CD8 Terminal effector	1684	2.1%	49.5%	9.3%	39.1%
C8: CD4 Unknown (a)	1195	27.7%	27.9%	29.1%	15.2%
C9: CD4 T regulatory	1041	17.9%	26.5%	35.7%	19.9%
C10: CD4 GPR25+	1000	20.8%	22.2%	19.0%	38.0%
C11: Mixed Terminally exhausted	989	13.9%	18.9%	36.6%	30.6%
C12: CD8 Naive	866	19.5%	36.3%	34.1%	10.2%
C13: CD8 MAIT-like	840	27.5%	34.4%	25.4%	12.7%
C14: CD8 Central memory	663	5.9%	51.6%	18.3%	24.3%
C15: CD4 Unknown (b)	658	24.6%	26.3%	28.6%	20.5%
C16: CD8 Progenitor exhausted	591	25.7%	5.4%	20.6%	48.2%
C17: CD8 Effector memory	586	10.4%	39.6%	19.6%	30.4%
C18: CD8 Innate-like effector	563	3.7%	9.8%	20.6%	65.9%
C19: CD8 iNKT-like	455	3.7%	12.7%	22.4%	61.1%
C20: Mixed Unknown	444	28.6%	32.7%	20.3%	18.5%
C21: Mixed Proliferating	244	21.7%	20.9%	36.5%	20.9%

CD44, CD28, and MHC-II molecules (DLA-DRA, DLA-DQA1) (Figure 3A). Notably, C6 is heterogenous in terms of e.g. GATA3 and CXCR3 expression (Figure 3B), indicating, that it contains recently activated T cells with different effector functions.

Two CD4-dominant clusters (C8, C15) were designated "unknown" CD4$^+$ T cells due to the lack of lineage-defining signature transcripts (Figure 3A). Increased expression of transcripts from mitochondrial genes in C8 may indicate clustering of cells with reduced viability, which could have resulted from freezing/thawing.

Interestingly, elevated expression of CD40LG, a cross-species marker of T helper cell (Th) activation by antigens (41–44), was detected in C5 (Th2) (Supplementary Table 2 and Figure 3D). Furthermore, a trend towards a higher expression level of CD40LG is observed in C6, supporting recent activation (Figure 3D).

3.3 Canine TCRαβ$^+$ CD8A-dominant clusters represent distinct differentiation states and include three innate-like subsets characterized by high expression of FCER1G

C12 comprises naïve CD8A$^+$ T cells that share a similar gene expression profile with the two naïve CD4 clusters C2 and C3 (LEF1, SELL, CCR7, TCF7) (Figures 3A, 4A), which are also located closely in the UMAP plot (Figure 2A). Furthermore, complement factor B (CFB) was found to be associated with canine TCRαβ$^+$ naïve CD4 and CD8A T cells (Figure 4B). Whereas naïve human CD8$^+$ T cells express KLRK1 encoding the activating NK receptor NKG2D (45), our data suggest activation-induced transcription in canine CD8$^+$ T cells (Figure 4A), that is also observed in mice (45).

Cells in C14, which were characterized by expression of CD7 and EOMES (Figure 4A), additionally showed elevated expression of the memory markers IL7R, CCR7, and CD28 when compared with all other CD8A-dominant clusters (Figure 4C and Supplementary Table 5), reminiscent of a central memory phenotype (46). Noteworthy, expression of SELL was not restricted to naïve and central memory CD8A clusters, but was also detected in CD8A clusters containing effector cells with high expression of cytotoxic molecules (C7, C13, C18) (Figures 4A, B). In contrast, CCR7 expression was found to be specifically associated with the naïve/central memory phenotype in CD8A-dominant clusters (C12, C14) (Figures 4B, C).

C17 expressed multiple effector transcripts (ZEB2$^+$, GZMB$^+$, GZMK$^+$, CCL4$^+$, and CCL5$^+$), consistent with effector memory CD8 T cells, while C7 showed a signature of terminally differentiated effector CD8 T cells (ZEB2$^+$, KLRG1$^+$, PRF1$^+$, FASLG$^+$GZMA$^+$, GZMB^{hi}, GZMK$^+$, CCL4^{hi}, CCL5$^+$) (Figure 4A).

Three innate-like T cell clusters (C13, C18, and C19) characterized by high expression of FCER1G were identified within

10.3389/fimmu.2023.1123366

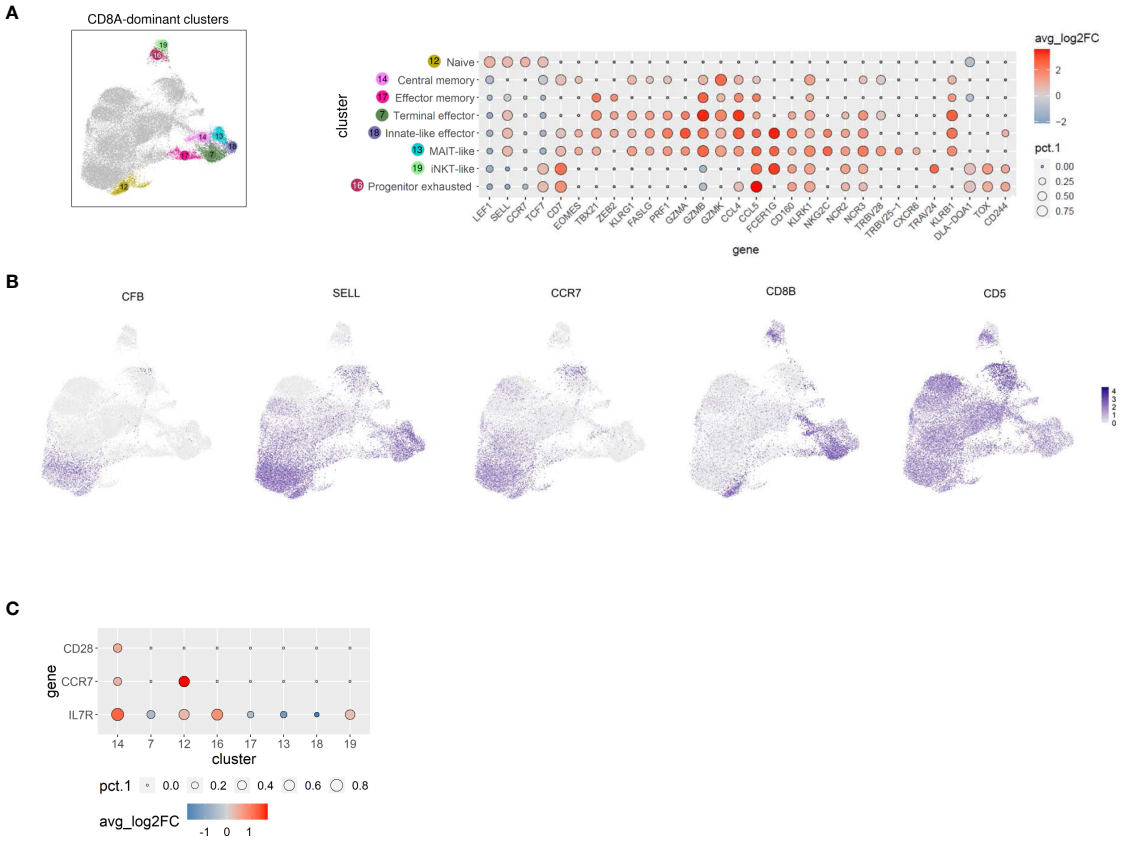

FIGURE 4
TCRαβ$^+$ CD8A-dominant clusters of the dog comprise distinct differentiation states and three innate-like subsets characterized by high expression of FCER1G, including a MAIT-like cell type. **(A)** CD8A-dominant clusters highlighted in UMAP plot were annotated based on expression of T cell subset marker genes shown in Dot plot. The dot size corresponds to the percentage (pct.1) of cells expressing the gene in each CD8A-dominant cluster, the color represents the expression level (average_log2 fold change). Genes were ordered to visualize the differences/similarities between cell types. **(B)** Expression of select genes across all canine TCRαβ$^+$ clusters visualized by FeaturePlots **(C)** Direct comparison of C14 with all other CD8A-dominant clusters confirms the assignment to central memory T cells.

the CD8A-dominant group (Figure 4A). Reduced expression of CD8B in these clusters (Figure 4B) supports their innate-like phenotype as murine and human CD8$^+$ innate-like T cells (i.e. MAIT cells, iNKT cells, and γδ T cells) show predominant expression of the CD8αα homodimer, in contrast to conventional T cell populations that are mainly CD8αβ$^+$ (47, 48). The transcription profile of C13 and C18 (but not C19) indicated high cytotoxic potential (FASLG$^+$, PRF1$^+$, GZMA$^+$, GZMB$^+$, GZMK$^+$) (Figure 4A). FCER1G provides necessary activation motifs for several NK receptors, including the natural cytotoxicity receptor 3 (NCR3) (49). However, expression of NCR3 was not restricted to FCER1G$^+$ clusters of canine TCRαβ$^+$ T cells (C13, C18, and C19) but was also detected in C7 (terminal effector CTL), C14 (central memory CTL), and C16 (progenitor exhausted, see below) (Figure 4A), probably due to different signal transduction pathways including FCER1G and/or CD3ζ adaptor molecules (49). Similarly, widespread expression of NCR2 encoding NKp44 was observed among CD8A-dominant clusters (Figure 4A). In contrast, NKG2C was only up-regulated in the two CD8$^+$ FCER1G$^+$ innate-like clusters with high cytotoxic potential (C13 and C18) (Figure 4A). Besides the similarities as compared to C18, C13 specifically showed upregulated expression of TRBV25-1, TRBV28, and CXCR6 (Figure 4A), indicating a mucosa-associated invariant T-cell (MAIT)-like phenotype (50, 51). Of note, V(D)J analysis confirmed a highly restricted T cell receptor repertoire of the MAIT-like cluster C13 (see below). C18 represents a population of canine CD8$^+$ FCER1G$^+$ ZEB2$^+$ innate-like effector cells (Figure 4A). The third FCER1G$^+$ innate-like cluster of canine TCRαβ$^+$ CD8A$^+$ T cells C19 was classified as iNKT-like due to elevated expression of TRAV24 but lack of typical cytotoxic effector molecules (Figure 4A). Down-regulated transcription of CD5 is another specific characteristic of the canine iNKT-like cell type (Figure 4A). Furthermore, enhanced expression of the MHC-II-encoding gene DLA-DQA1 as well as absence of KLRB1 expression was detected in cells of this cluster (Figure 4A). In humans, this iNKT-phenotype is associated with exhaustion and decreased expression of cytotoxic factors (52). Accordingly, canine iNKT-like cells showed an elevated transcription level of TOX (Figure 4A), known to promote the generation of exhausted T cells while repressing development of the KLRG1$^+$ T effector cell lineage (53–55). Cluster C16 differs from the iNKT-like cluster C19 in terms of FCER1G and TRAV24 expression but shows a similar progenitor exhausted T cell profile with upregulated transcription of TOX, TCF7 (encoding the transcription factor TCF-1), and CD244 (encoding the inhibitory receptor 2B4) and downregulated effector genes, including ZEB2, KLRG1, GZMA, GZMB, GZMK, PRF1, and FASLG (53–55). Furthermore, C16 (progenitor exhausted) shows highest expression

of CXCR3 among CD8A-dominant clusters and constitutive expression of IFNG (Figure 3B; compare Figure 4A for cluster location of C16).

Taken together, scRNA-seq revealed new insights into the heterogeneity of canine TCRαβ$^+$ T cells and led to the first identification of CD8$^+$ FCER1G$^+$ innate-like T cell populations in dogs, including a MAIT-like and an innate effector-like cell type, both with high cytotoxic potential as well as an iNKT-like cell type with features of exhaustion.

3.4 TCRαβ$^+$ CD4/CD8A-mixed clusters of the dog include terminally exhausted and proliferating cells

Significantly upregulated expression of PDCD1 encoding programmed cell death protein-1 (PD-1) was exclusively found in C11 (Supplementary Table 2), representing a CD4/CD8A-mixed cluster (Figure 2C). Thus, C11 is likely to comprise canine TCRαβ$^+$ terminally exhausted CD4 and CD8 T cells (Figure 5). Due to the lack of lineage-defining signature transcripts, C20 was designated "unknown" CD4/CD8A-mixed population. Cells of this cluster express comparatively low levels of naïve markers (LEF1, SELL, TCF7, CCR7) as well as of activation markers (e.g. CD44) (Figure 5 and Supplementary Table 2). Cells in C21 uniquely expressed numerous cell cycle-related genes, such as MKI67, PCLAF, TOP2A, CLSPN, and KIF15, and accordingly C21 contains proliferating TCRαβ$^+$ T cells (Figure 5 and Supplementary Table 2).

3.5 Canine iNKT-like cells frequently have more than one TRA rearrangement

The T cell receptor repertoire was characterized for all clusters identified by transcriptome analysis. As expected, the majority of cells had one productive TRA and TRB rearrangement each (16,603 cells, 62.1%) followed by cells with either one productive TRB rearrangement only (5,640 cells, 21.1%) or one productive TRA rearrangement only (2,337, 8.7%) (Supplementary Table 6). The medium percentage of cells for which at least one rearrangement could be detected was 87.4% with 17/22 clusters showing TCR rearrangements in at least 75% of cells (Figure 6). Some clusters comprised a disproportionate number of cells with more than two rearrangements. In the CD8A-dominant iNKT-like cluster, 26.6% of cells had 2xTRA/1xTRB rearrangements (median percentage across all clusters 3.8%). Furthermore, in the CD4-dominant cluster C15, designated "unknown (b)" (Figure 3A), 21.7% of cells had 1xTRA/2xTRB rearrangements (median percentage across all clusters 1.7%) and 9.7% of cells had 2xTRA/2xTRB rearrangements (median percentage across all clusters 0.5%) (Figure 6). For the dog, this is the first indication of dual TCR expression, previously observed in murine and human studies (56).

3.6 MAIT-like and iNKT cells have a skewed TRA junctional length

Considering cells with a single TRA and TRB rearrangement each, the junctional length of TRA and TRB rearrangements was normally distributed for most clusters with a median length of 14 and 15 amino acids (aa), respectively (Figure 7 and Supplementary Figure 3). Clusters with a skewed junctional length were the MAIT-like cluster (C13), which had a markedly restricted TRA junctional length at 16 aa, as well as the iNKT-like cluster (C19) with a dominant TRA junctional length of 13 amino acids (Figure 7 and Supplementary Figure 3). MAIT-like cells had a slight bias toward 12 aa and 14 aa in the TRB repertoire, but overall, the TRB junctional length was less skewed than the TRA junctional length. Since TRA rearrangements are not routinely assessed in dogs, these data provide the first evidence for invariant T cell receptors in dogs.

3.7 TRAV9-11 is preferentially used in FCER1G$^+$ innate-like CD8A T cell subsets and rearranges almost exclusively to TRAJ28 in MAIT-like cells

The most frequently used TRAV gene families were TRAV43 and TRAV9 with the top 3 TRAV genes having a median percent usage of 14.4% (TRAV43-1), 8.9% (TRAV9-6), and 8.3% (TRAV43-4) across 22 clusters (Figure 8). A clear outlier was TRAV9-11, which was used in 82.5% of MAIT-like cells (C13), 35.4% of innate-like effector cells (C18) and 28.2% of effector memory cells (C17) of the CD8A-dominant group. The TRAJ usage was generally evenly distributed with the three most frequently used genes TRAJ33, TRAJ52 and TRAJ28 accounting for 4-5% of rearrangements. However, analogous

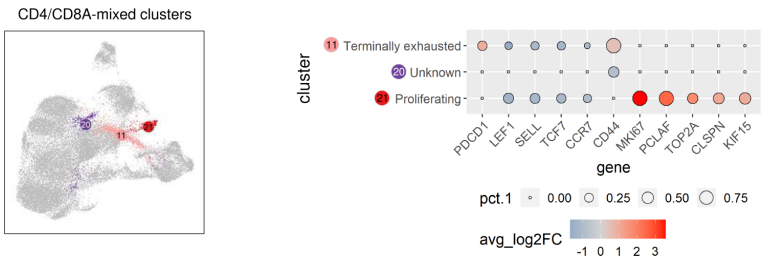

FIGURE 5
TCRαβ$^+$ CD4/CD8A-mixed clusters of the dog include terminally exhausted and proliferating cells. CD4/CD8A-mixed clusters highlighted in UMAP plot were annotated based on expression of signature genes shown in Dot plot. The dot size corresponds to the percentage (pct.1) of cells expressing the gene in each CD4/CD8A-mixed cluster, the color represents the expression level (average_log2 fold change).

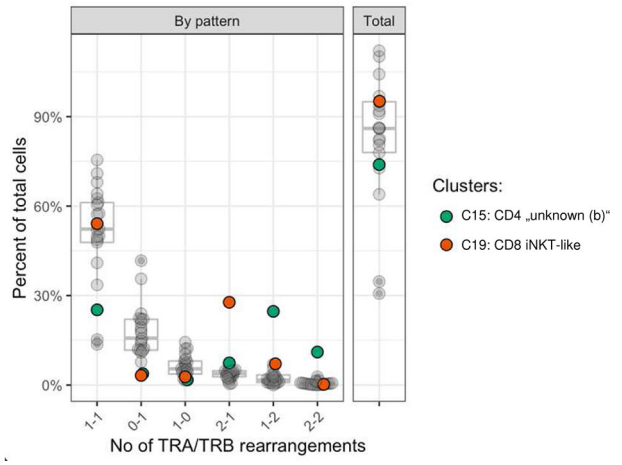

FIGURE 6
Frequency of TRA/TRB rearrangement patterns per cell stratified by cluster. Most cells had one TRA and one TRB rearrangement (median 52.1%). Cells with 2xTRA/1xTRB rearrangements were more common in the CD8A-dominant iNKT-like cluster (C19, red) and cells with either 1xTRA/2xTRB rearrangements or 2xTRA/2xTRB rearrangements were more common in the CD4-dominant "unknown" (b) cluster (C15, green). x-axis: number of TRA and TRB rearrangements per cell, format: 'x-y'; x: number of TRA rearrangements; y: number of TRB rearrangements per cell; example: '2-1': cells with 2 TRA rearrangements and 1 TRB rearrangement; y-axis: percent of cells out of all cells.

to TRAV genes, MAIT-like cells (C13) showed a strong bias utilizing TRAJ28 in 87.7% of cells.

When assessing V/J pairing, 82.1% of MAIT-like cells (C13) and 21.2% of effector memory cells (C17) of the CD8A-dominant group utilized TRAV9-11 rearranged to TRAJ28 (Figure 9). In CD8A innate-like effector cells (C18), the dominant V gene TRAV9-11 also rearranged to TRAJ28 (15.1% of cells) but additionally paired with TRAJ20 at slightly higher frequency (16.8% of cells). In iNKT-like cells (C19), the two dominant V genes TRAV43-1 and TRAV24 rearranged to a variety of different J genes, suggesting a less restricted pairing pattern in this subset.

3.8 FCER1G^{+} innate-like CD8A T cells have variable diversification of TRA junctional regions

Given the disproportionate use of TRAV9-11 in MAIT-like (C13), innate-like effector (C18), and effector memory (C17) cells of the CD8A-dominant group we further explored the junctional sequence in these clusters. Most cells had a junctional length of 16 amino acids (568 cells, 92.1%) and, except for amino acid positions 4-6, an invariant junctional sequence with the motif 'CAL…YSGVGSQLTF' (Figure 9). This was a consistent finding in all 3 examined clusters and, at least for MAIT-like cells (C13), was true for all 4 dogs. Out of the 16 aa positions, 10 were encoded by the J gene, 4 by the V gene, and 2 were added nucleotides. A subset of CD8A-dominant innate-like effector cells (C18) had a junctional length of 12 amino acids (49 cells, 7.7%). The subset of CD8A-dominant innate effector cells (C18) with a junctional length of 12 amino acids (7.7%) likely reflects a single expanded clone, as it was found only in dog 4, was supported by only 49 cells, and had a single junctional sequence (motif 'CALSDLSYNYIF').

3.9 TRB repertoire bias is most common in MAIT-like and iNKT-like cells but is less pronounced than in TRA

The 3 most frequently utilized TRBV genes were TRBV16 (14.9%), TRBV7 (11.9%), and TRBV18 (10.2%) (Figure 10A). Clusters with a strongly biased gene usage were the MAIT-like cluster (C13) utilizing TRBV28 in 30.7% and TRBV25 in 30.2% of cells and the iNKT-like cluster (C19) utilizing TRBV26 in 27.9% of cells. Owing to a smaller number of J genes, the median TRBJ gene

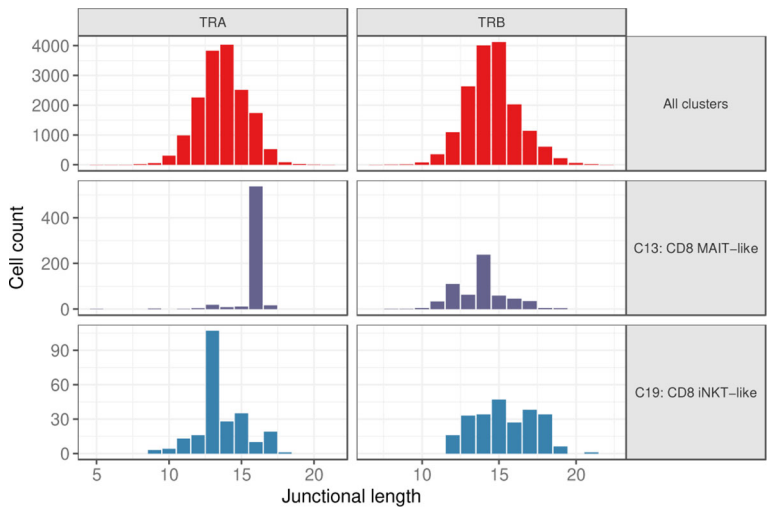

FIGURE 7
Junctional length of TRA and TRB rearrangements for all clusters combined (top), the MAIT-like cluster (C13) (middle), and the iNKT-like cluster (C19) (bottom).

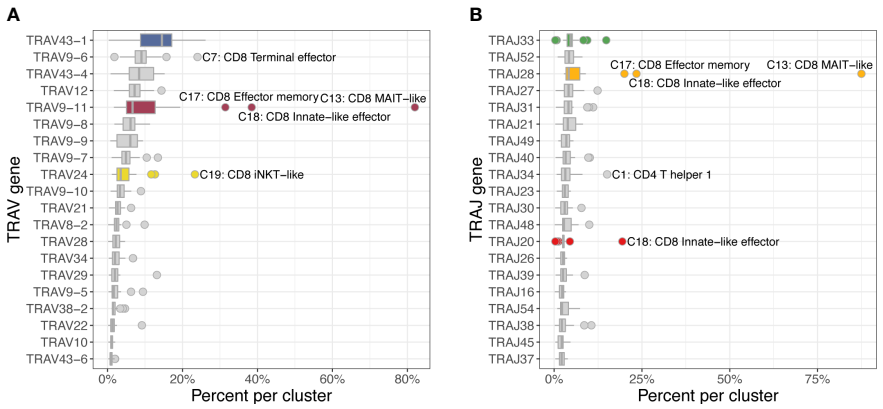

FIGURE 8
Usage frequencies of the 20 most common TRAV genes **(A)** and TRAJ genes **(B)** showing usage bias for several subsets of the CD8A-dominant group (CD8). TRAV9-11 was more frequently used in MAIT-like cells (C13) and, to a lesser degree, in innate-like effector (C18) and effector memory (C17) cells. TRAJ28 was disproportionally utilized in MAIT-like cells (C13).

usage was generally higher than that of TRAJ genes with TRBJ2-6, TRBJ2-1, and TRBJ1-2 used in 15.2%, 14.8%, and 11.1% of clusters, respectively (Figure 10B). Cells utilizing a TRBJ2 gene were slightly more abundant than cells using a TRBJ1 gene (44.1% vs. 55.9%). Disproportionately used TRBJ genes were TRBJ2-1 in iNKT-like cells (26.1%) and TRBJ2-5 in MAIT-like cells (25.0%). The V/J gene pairing for TRB sequences was a lot less restricted than observed for TRA (Figure 11). Any given TRB V gene rearranged to multiple different J genes at similar frequencies.

3.10 A MAIT-like dominated TRA supercluster is characterized by large size, high centrality and high publicity

To characterize repertoire overlap across T cell subsets and dogs, we clustered clonotypes with similar amino acid sequence. The TRA repertoire had a lower number of unique junctional sequences (clonotypes) (n=9,542) but a markedly higher number of clusters (n=985) as compared to the TRB repertoire (11,150 clonotypes; 168 clusters) (Figure 12A). For TRA, cluster # 2422 (TRAV9/TRAJ28) stood out because it had the most cells (n=625), the most clonotypes (n=144), the highest centrality and the greatest cluster density (Figure 12A). Furthermore, this cluster was predominantly comprised of MAIT-like cells (C13) and, to a lesser degree, innate-like effector cells (C18) of the CD8A-dominant group (Figure 12B). In contrast, other dominant clusters consisted of multiple T cell subsets that were mostly of CD4 lineage (data not shown). For TRB, cluster #3273 had the highest centrality and cluster density (Figure 12A), however, all metrics were significantly lower than those of TRA cluster # 2422. While 16.5% of TRA clusters were comprised of clonotypes from all 4 dogs, no TRB cluster had sequences from more than 3 dogs (Figure 12A). TRB clusters with clonotypes from 3 dogs only comprised 4.2% of all clusters (Figure 12A). When assessing the composition of clusters with respect to T cell subset, cluster #2422 stood out because it was primarily composed of CD8 MAIT-like cells (Figures 12B, C). Visualizing clonal relationships using network plots, we found that certain clonotypes occurred in more than one T-cell subset (Figure 12C), were unique to one dog or were shared by multiple dogs (Figure 12D), and were extremely related with up to 25 sequences that differed by a single amino acid only (Figure 12E). The sequence variability was restricted to amino acid positions 4-6 (Figures 12F, G). When comparing repertoire overlap across T cell subsets, we found the greatest overlap between subsets of the CD4-dominant group, specifically T central memory (C0), naïve (a) (C2) and naïve (b) (C3) cells (Supplementary Figure 4). The CD8A-dominant MAIT-like subset shared the least overlap with other T cell subsets (Supplementary Figure 4), despite harboring the largest cluster (Figure 12).

4 Discussion

Given the value of the dog as a model species for various human disorders (including autoimmune diseases, allergy, and cancer), a better understanding of canine T cells could support in-depth mechanistic analyses in these models and might reveal novel targets for immunotherapy. Here, we use 5' scRNA-seq combined with immune repertoire sequencing to resolve TCR$\alpha\beta^+$ T cell populations of healthy dogs at an unprecedented resolution. The resulting T cell atlas of canine peripheral blood sheds new light into the diversity of these critical immune cells. Among the 22 annotated clusters were several CD4 and CD8A T cell populations not previously described in dogs. Of note, high expression of FCER1G identified three populations of canine innate-like CD8A$^+$ T cells in peripheral blood, showing a MAIT-like, an innate effector-like, and an iNKT-like phenotype, respectively. Expression of FCER1G has been shown to be associated with human innate T cells, comprising MAIT cells, iNKT cells and γδ T cells (57). These cells exhibit innate characteristics during inflammation and infection, such as rapid activation kinetics without prior pathogen exposure, and the capacity for TCR-independent activation by inflammatory cytokines such as IL-12, IL-18, and type I interferons (57–60). Expression of gene products responsible for effector functions such as cytotoxicity and cytokine production is a hallmark of human innate T cells (57). In the current study, high cytotoxic potential was observed in the MAIT-

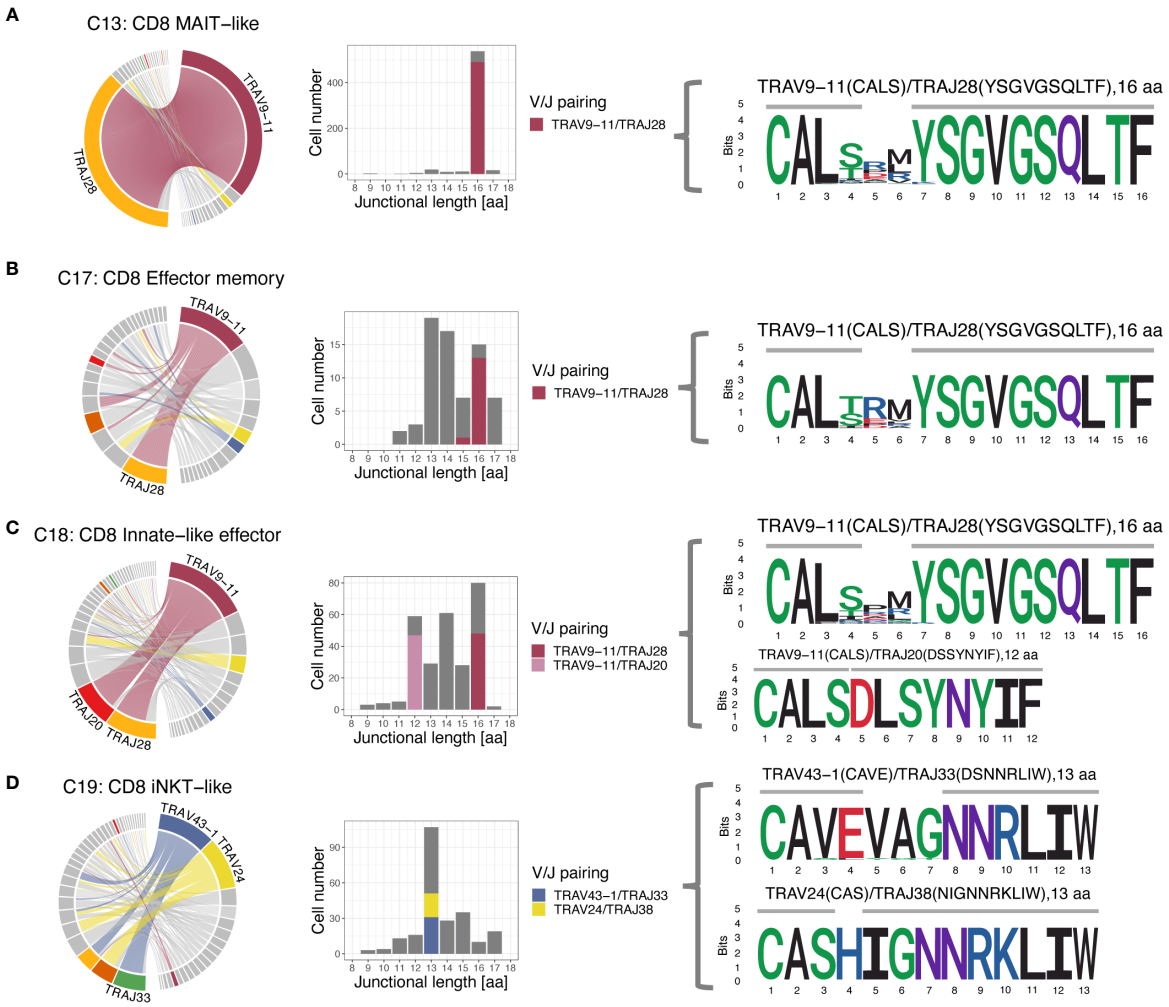

FIGURE 9
T cell receptor alpha (TRA) V/J pairing (left), junctional length (middle) and junctional sequence (right) of 4 clusters with skewed V/J usage. **(A-C)** The MAIT-like cluster (C13), and to a lesser degree, the effector memory (C17) and innate-like effector (C18) clusters all have a dominant TRAV9-11/TRAJ28 rearrangement with 16 aa junctional length and the CDR3 is mostly germline encoded with two amino acids added. **(C)** The TRAV9-11 gene in the innate-like cluster (C18) additionally rearranges to TRAJ20 with 12 aa junctional length, which is entirely germline encoded and has no added bases. **(D)** The iNKT-like cluster (C19) predominantly uses the V genes TRAV43-1 and TRAV24, which rearrange to a number of different J genes. While 13 aa length sequences dominate, the junctional sequences are more diverse than sequences utilizing TRAV9-11 in the other 3 clusters and show more evidence of deletions and additions. Left column: chord diagram displaying V/J pairing; Middle column: junctional length; dominant V/J pairings are highlighted; Right column: position weight matrix of junctional sequence; horizontal grey bar indicates the extent of the germline variable (right) and joining (left) genes.

like as well as in the CD8A$^+$ innate effector-like cell populations. Of note, innate effector-like T cells may be interesting candidates for novel cancer treatment strategies. Recently, FCER1G$^+$ NK1.1$^+$ innate-like TCRαβ$^+$ T cells with high cytotoxic potential have been identified in murine and human malignancies. Activation of IL-15 signaling in corresponding murine progenitor cells was shown to suppress tumor-growth *in vivo* after adoptive transfer (61). Furthermore, a population of IL-15-induced human circulating NKp30$^+$FcεR1γ$^+$ CD8$^+$ T cells was described to exhibit high NK-like anti-tumor activity *in vitro* and in a preclinical xenograft mouse model *in vivo* (62). FCER1G-dependent upregulation of NK receptors may potentiate rapid acquisition of effector functions of innate-like T cells in tumor tissues (61). Interestingly, in the present study we found widespread expression of several NK receptors among canine CD8A$^+$ T cells, including the FCER1G$^+$ populations. Our data provide an important reference for future studies evaluating T cell responses in canine diseases. This also applies, for example, to the newly identified canine TOX$^+$TCF7$^+$ progenitor-like exhausted T cell population (C16). Exhausted CD8$^+$ T cells are the major target of checkpoint blockade in patients with cancer and modulation of TOX, a transcription factor required for epigenetic remodeling and survival of functionally impaired exhausted T cells, has been suggested as a potential target for immunotherapy (63). It needs to be studied, whether TOX$^+$ TCF7$^+$ progenitor-like exhausted T cells are enriched in tumors of dogs.

The integration of immune repertoire sequencing into the single cell RNA seq workflow enabled the discovery of MAIT-like T cells in dogs. Similar to MAIT cells of other species (64), the newly identified MAIT-like cell population in dogs expresses an invariant TCR-α chain characterized by a distinct TRAV/TRAJ gene usage and a constant junctional length, paired with a TCR-β chain using a limited number of TRBV genes. Interestingly, dogs lack the

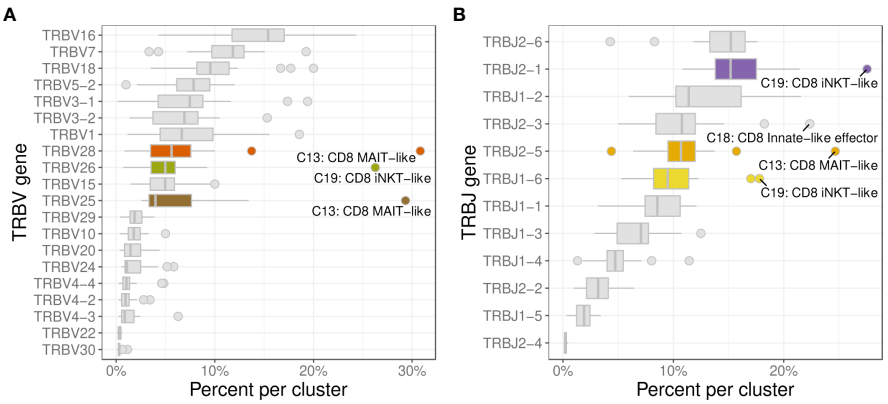

FIGURE 10
Usage frequencies of the most common TRBV genes **(A)** and TRBJ genes **(B)** showing usage bias for MAIT-like cells (C13), and iNKT-like cells (C19).

nonclassical MHC-I-like molecule MR1, which presents microbial riboflavin precursor derivatives to MAIT cells in most mammals, as well as the TRAV1 gene, the canonical TRAV gene used in these cells (64). Instead, canine MAIT-like cells show preferential usage of the TRAV9-11 gene. Thus, the kind of antigens recognized by MAIT-like cells of dogs as well as the mechanism of antigen presentation are exciting questions for future studies.

Similar to MAIT-like cells, canine FCER1G^{+} innate-like iNKT-like cells, showed a biased TRA repertoire with a restricted junctional length but two different dominant V genes, TRAV24 and TRAV43-1. In a previous study, a canine CD3^{+} T cell population reactive to α-galactosylceramide (α-Gal-Cer)-loaded mouse CD1d has been suggested to represent iNKT cells of the dog with homology of the variable and joining regions of the TCRα-chain to both, mouse Vα14-Jα281 and human Vα24-JαQ (65). However, CD1d, the non-classical MHC class-I-related molecule presenting (glyco)lipid antigens to iNKT cells in various species, is likely non-functional in dogs (66, 67). Thus, whether dogs utilize an alternative MHC-I-like molecule than CD1d presenting a distinct set of antigens to the newly identified innate-like iNKT-like population, needs further investigation. In humans, the MHC-II^{+}KLRB1^{-} phenotype of iNKT cells is not only associated with decreased expression of cytotoxic molecules, which was also observed in this study for dogs but additionally with a Th1-skewed cytokine profile (52). In future studies, scRNA-seq analysis following stimulation could provide further insights into cytokine-producing capabilities and functional properties of the various TCRαβ^{+} T cell subpopulations of

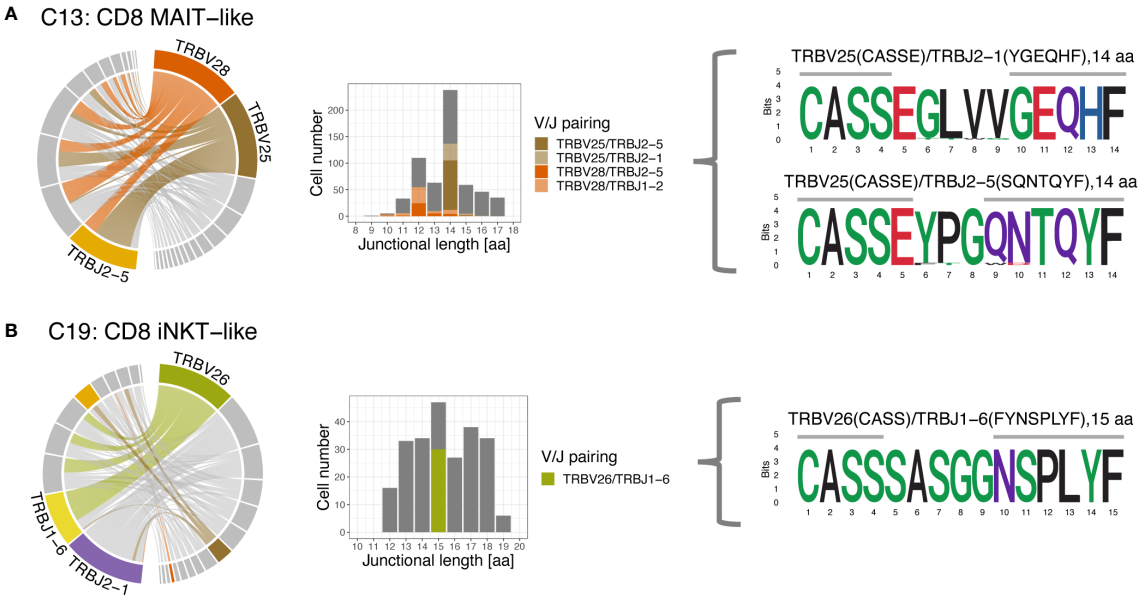

FIGURE 11
T cell receptor beta (TRB) V/J pairing (left), junctional length (middle) and junctional sequence (right) of two clusters with skewed V/J usage. **(A)** The MAIT-like cluster predominantly uses TRBV25 and TRBV28, which rearrange to a variety of J genes. Rearrangements involving TRBV25 and TRBV28 mostly have a junctional length of 14 and 12 aa, respectively. **(B)** The iNKT-like cluster preferentially uses TRBV26 and rearranges to various J genes. Rearrangements utilizing TRBV26 have variable junctional length; note low coverage for this cluster. Left column: chord diagram displaying V/J pairing; Middle column: junctional length; dominant V/J pairings are highlighted; Right column: position weight matrix of junctional sequence; horizontal grey bar indicates the extent of the germline variable (right) and joining (left) genes.

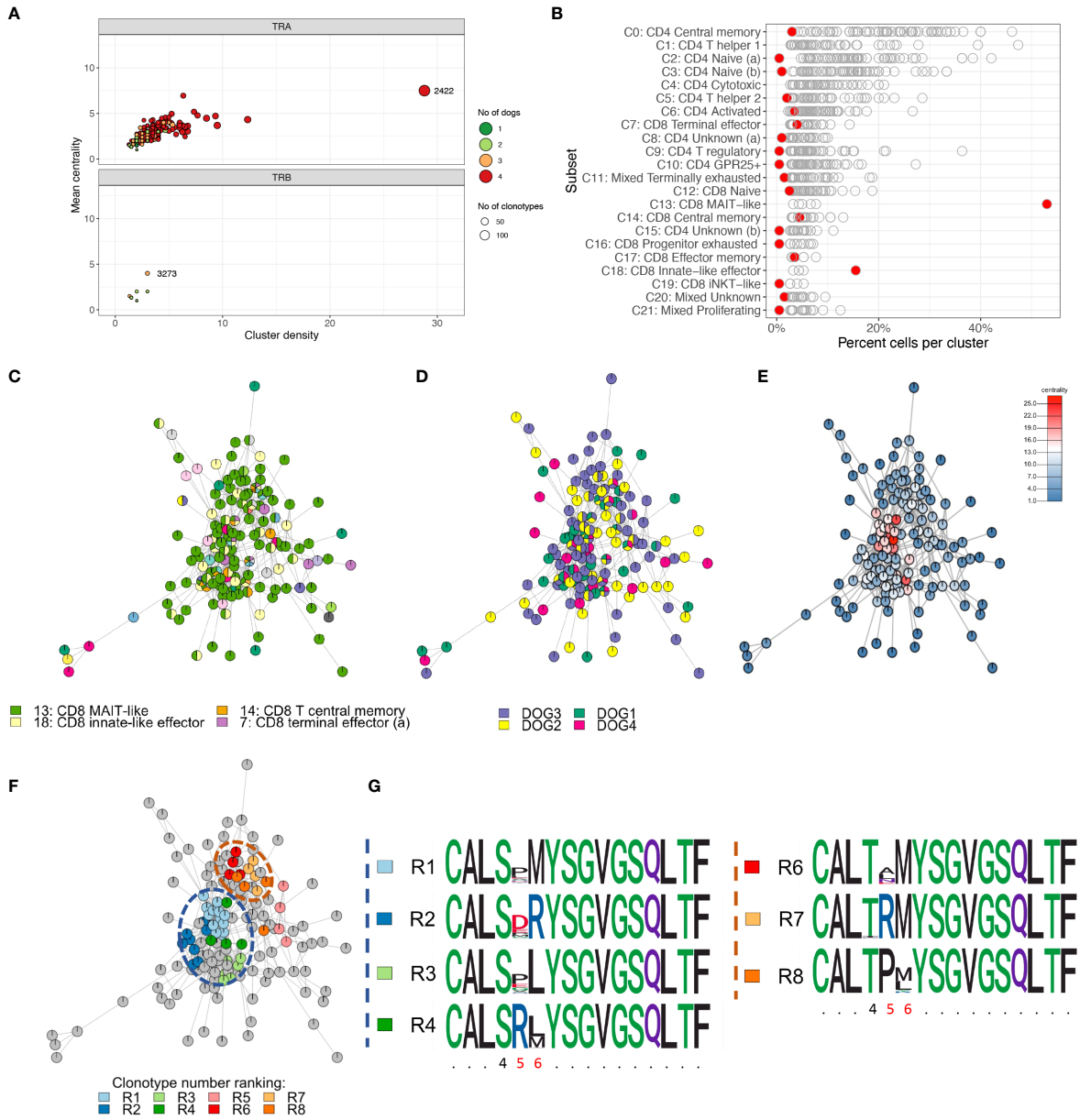

FIGURE 12
Cluster analysis identifying closely related clonotypes across T cell subsets and dogs. **(A)** Cluster summary. TRA cluster #2422 stands out because it comprises the most unique clonotypes, the highest cluster density and centrality and comprises sequences from all four dogs (top). There are markedly fewer TRB clusters than TRA clusters. TRB clusters contain fewer clonotypes, have a lower cluster density and centrality and comprise sequences from at most three dogs. **(B)** Cluster composition by T cell subset. Each point is one cluster, cluster #2422 is highlighted red. MAIT-like cells (C13) are overrepresented in cluster #2422; iNKT-like cells (C19) are not enriched. **(C-F)** Network plots of 'relatedness' of clonotypes in TRA cluster #2422 highlighting different variables of interest. All clonotypes that differ by one amino acid are connected by edges. Pie chart notes depict the relative frequency of values for a given variable. **(C)** T cell subsets. MAIT-like cells (green) are dominant; certain clonotypes are seen in multiple different subsets. **(D)** Dogs. The degree of 'publicity' of clonotypes ranges from unique for a given clonotype to shared by all four dogs; **(E)** Centrality. The centrality rank reflects the number of edges for a given node. The high ranking clonotypes in the central areas of the cluster are indicative of a high 'density' of closely related sequences; **(F)** Sub-clusters derived by complete linkage (cl) clustering highlighting the most closely related sequences. All clonotypes within a given cl cluster differ by a single amino acid only; the top-ranking cl clusters based on clonotype abundance (rank R1-R8) are colored. **(G)** Dissecting the sequence composition of cl clusters highlighted in **(F)** using position weight matrixes. Two groups of cl clusters (blue and orange dashed circle) are highly variable in positions 5 and 6 and have either a serine (S) (blue group) or threonine (T) (orange circle) in position 4. x-axis: amino acid position, invariable positions are abbreviated with a period, variable positions within a cl cluster are highlighted red.

dogs. This is expected to also reveal a cluster of $CD4^+$ Th17 cells. In the present study, the master transcription factor of Th17 cells (encoded by RORC), as well as other Th17 cell-related molecules (STAT3, CCR6, RORA, IL23R, IL17A) were not found to be differentially expressed between clusters (data not shown). The combined analysis of transcriptome and immune repertoire of $TCR\alpha\beta^+$ T cells established in this study can be also used in further experiments to characterize tissue-specific expression of effector and regulatory molecules as well as potentially distinct TCR repertoires of circulating vs. tissue-resident T cells, including Treg cells.

Canine $TCR\alpha\beta^+$ T cells comprise a fraction of ~15% non-conventional $CD4^-CD8\alpha^-$ double-negative (14) as well as a small

fraction of non-conventional $CD4^+CD8\alpha^+$ double-positive T cells (68–70). Double-negative T cells were excluded from analysis in the present study since it was not possible to discriminate between true double-negative T cells and double-negative T cells resulting from drop-out of CD4, a phenomenon already observed previously (5, 13). This could also have resulted in an underestimation of $CD4^+CD8A^+$ dp T cells. Single cell RNA-seq of sorted dn/dp $TCR\alpha\beta^+$ T cells in future experiments would allow for comparison of gene expression patterns of these non-conventional populations with conventional single-positive T cells. Of note, presence of well-known T helper cell and Treg cell clusters in the CD4-dominant group supports the classification used in the present study.

Taken together, this study contributes to a better understanding of the cellular diversity of peripheral blood $TCR\alpha\beta^+$ T cells providing a basis to inform translational efforts in the field of immunotherapy.

Data availability statement

The data presented in the study are deposited in the NCBI GEO repository, accession number GSE218355.

Ethics statement

The animal study was reviewed and approved by Saxony State Office (Landesdirektion Sachsen) in Leipzig, Germany (approval number: DD24.1-5131/444/30).

Author contributions

ME, GA, and SK designed experiments and wrote the manuscript. ME and SK performed experiments. PM provided key reagents. HC performed the TCR (TRA, TRB) cluster analysis. All authors contributed to the article and approved the submitted version.

Funding

This study was funded by grant ES 645/1-1 (to ME) from the German Research Foundation (Deutsche Forschungsgemeinschaft, DFG) and by the Open Access Publishing Fund of Leipzig University supported by the German Research Foundation within the program Open Access Publication Funding.

Acknowledgments

Special thanks go to Anett Grohs for her excellent technical assistance. Dr. Christiane Schnabel, Dr. Uwe Müller, and Dr. Mathias Büttner are thanked for critical reading of the manuscript. Dr. Uwe Müller is kindly acknowledged for his support in creating Figure 1A using BioRender.com. Flow cytometry was performed at the Core Unit Flow Cytometry (CUDZ) of the College of Veterinary Medicine, University of Leipzig. The sequencing was carried by the DNA Technologies and Expression Analysis Core at the UC Davis Genome Center, supported by NIH Shared Instrumentation Grant 1S10OD010786-01. We thank the UC Davis Bioinformatics Core for their services in data analysis. The authors thank Ina Hochheim and Caroline Schöller from the Institute of Pharmacology, Pharmacy and Toxicology, College of Veterinary Medicine, University of Leipzig for providing blood samples and extensive care of the dogs.

Conflict of interest

The authors declare that the research was conducted in the absence of any commercial or financial relationships that could be construed as a potential conflict of interest.

Publisher's note

Supplementary material

The Supplementary Material for this article can be found online at: https://www.frontiersin.org/articles/10.3389/fimmu.2023.1123366/full#supplementary-material

References

1. Gershwin LJ. Veterinary autoimmunity: Autoimmune diseases in domestic animals. *Ann N Y Acad Sci* (2007) 1109:109–16. doi: 10.1196/annals.1398.013

2. Mueller RS, Jensen-Jarolim E, Roth-Walter F, Marti E, Janda J, Seida AA, et al. Allergen immunotherapy in people, dogs, cats and horses - differences, similarities and research needs. *Allergy* (2018) 73:1989–99. doi: 10.1111/all.13464

3. Overgaard NH, Fan TM, Schachtschneider KM, Principe DR, Schook LB, Jungersen G. Of mice, dogs, pigs, and men: Choosing the appropriate model for immuno-oncology research. *ILAR J* (2018) 59:247–62. doi: 10.1093/ilar/ily014

4. Nayak R, Hasija Y. A hitchhiker's guide to single-cell transcriptomics and data analysis pipelines. *Genomics* (2021) 113:606–19. doi: 10.1016/j.ygeno.2021.01.007

5. Patel RS, Tomlinson JE, Divers TJ, van de Walle GR, Rosenberg BR. Single-cell resolution landscape of equine peripheral blood mononuclear cells reveals diverse cell types including T-bet+ b cells. *BMC Biol* (2021) 19:13. doi: 10.1186/s12915-020-00947-5

6. Fastrès A, Pirottin D, Fievez L, Marichal T, Desmet CJ, Bureau F, et al. Characterization of the bronchoalveolar lavage fluid by single cell gene expression analysis in healthy dogs: A promising technique. *Front Immunol* (2020) 11:1707. doi: 10.3389/fimmu.2020.01707

7. Stubbington MJ, Rozenblatt-Rosen O, Regev A, Teichmann SA. Single-cell transcriptomics to explore the immune system in health and disease. *Science* (2017) 358:58–63. doi: 10.1126/science.aan6828

8. Chen D, Sun J, Zhu J, Ding X, Lan T, Wang X, et al. Single cell atlas for 11 non-model mammals, reptiles and birds. *Nat Commun* (2021) 12:7083. doi: 10.1038/s41467-021-27162-2

9. Butler A, Hoffman P, Smibert P, Papalexi E, Satija R. Integrating single-cell transcriptomic data across different conditions, technologies, and species. *Nat Biotechnol* (2018) 36:411–20. doi: 10.1038/nbt.4096

10. Stuart T, Butler A, Hoffman P, Hafemeister C, Papalexi E, Mauck WM, et al. Comprehensive integration of single-cell data. *Cell* (2019) 177:1888–1902.e21. doi: 10.1016/j.cell.2019.05.031

11. Zappia L, Oshlack A. Clustering trees: a visualization for evaluating clusterings at multiple resolutions. *Gigascience* (2018) 7:1–9. doi: 10.1093/gigascience/giy083

12. Cunningham F, Achuthan P, Akanni W, Allen J, Amode MR, Armean IM, et al. Ensembl 2019. *Nucleic Acids Res* (2019) 47:D745–51. doi: 10.1093/nar/gky1113

13. Wang X, Shen X, Chen S, Liu H, Hong N, Zhong H, et al. Reinvestigation of classic T cell subsets and identification of novel cell subpopulations by single-cell RNA sequencing. *J Immunol* (2022) 208:396–406. doi: 10.4049/jimmunol.2100581

14. Rabiger FV, Rothe K, von Buttlar H, Bismarck D, Büttner M, PF M, et al. Distinct features of canine non-conventional CD4-CD8α- double-negative TCRαβ+ vs. *TCRγδ+ T Cells Front Immunol* (2019) 10:2748. doi: 10.3389/fimmu.2019.02748

15. Niu N, Qin X. New insights into IL-7 signaling pathways during early and late T cell development. *Cell Mol Immunol* (2013) 10:187–9. doi: 10.1038/cmi.2013.11

16. Jurgens AP, Popović B, Wolkers MC. T Cells at work: How post-transcriptional mechanisms control T cell homeostasis and activation. *Eur J Immunol* (2021) 51:2178–87. doi: 10.1002/eji.202049055

17. Huang GN, Huso DL, Bouyain S, Tu J, McCorkell KA, May MJ, et al. NFAT binding and regulation of T cell activation by the cytoplasmic scaffolding homer proteins. *Science* (2008) 319:476–81. doi: 10.1126/science.1151227

18. Kerdiles YM, Beisner DR, Tinoco R, Dejean AS, Castrillon DH, DePinho RA, et al. Foxo1 links homing and survival of naive T cells by regulating l-selectin, CCR7 and interleukin 7 receptor. *Nat Immunol* (2009) 10:176–84. doi: 10.1038/ni.1689

19. Yánez DC, Ross S, Crompton T. The IFITM protein family in adaptive immunity. *Immunology* (2020) 159:365–72. doi: 10.1111/imm.13163

20. Rice JM, Zweifach A, Lynes MA. Metallothionein regulates intracellular zinc signaling during CD4(+) T cell activation. *BMC Immunol* (2016) 17:13. doi: 10.1186/s12865-016-0151-2

21. Baldauf H-M, Pan X, Erikson E, Schmidt S, Daddacha W, Burggraf M, et al. SAMHD1 restricts HIV-1 infection in resting CD4(+) T cells. *Nat Med* (2012) 18:1682–7. doi: 10.1038/nm.2964

22. Nish SA, Zens KD, Kratchmarov R, Lin W-HW, Adams WC, Chen Y-H, et al. CD4 + T cell effector commitment coupled to self-renewal by asymmetric cell divisions. *J Exp Med* (2017) 214:39–47. doi: 10.1084/jem.20161046

23. Sallusto F, Geginat J, Lanzavecchia A. Central memory and effector memory T cell subsets: function, generation, and maintenance. *Annu Rev Immunol* (2004) 22:745–63. doi: 10.1146/annurev.immunol.22.012703.104702

24. Biassoni R, Cantoni C, Pende D, Sivori S, Parolini S, Vitale M, et al. Human natural killer cell receptors and co-receptors. *Immunol Rev* (2001) 181:203–14. doi: 10.1034/j.1600-065X.2001.1810117.x

25. Chiossone L, Vienne M, Kerdiles YM, Vivier E. Natural killer cell immunotherapies against cancer: Checkpoint inhibitors and more. *Semin Immunol* (2017) 31:55–63. doi: 10.1016/j.smim.2017.08.003

26. Cenerenti M, Saillard M, Romero P, Jandus C. The era of cytotoxic CD4 T cells. *Front Immunol* (2022) 13:867189. doi: 10.3389/fimmu.2022.867189

27. Oh DY, Fong L. Cytotoxic CD4+ T cells in cancer: Expanding the immune effector toolbox. *Immunity* (2021) 54:2701–11. doi: 10.1016/j.immuni.2021.11.015

28. Alonso-Arias R, Moro-García MA, López-Vázquez A, Rodrigo L, Baltar J, García FM, et al. NKG2D expression in CD4+ T lymphocytes as a marker of senescence in the aged immune system. *Age (Dordr)* (2011) 33:591–605. doi: 10.1007/s11357-010-9200-6

29. Hashimoto K, Kouno T, Ikawa T, Hayatsu N, Miyajima Y, Yabukami H, et al. Single-cell transcriptomics reveals expansion of cytotoxic CD4 T cells in supercentenarians. *Proc Natl Acad Sci USA* (2019) 116:24242–51. doi: 10.1073/pnas.1907883116

30. Xu D, Chan WL, Leung BP, Hunter D, Schulz K, Carter RW, et al. Selective expression and functions of interleukin 18 receptor on T helper (Th) type 1 but not Th2 cells. *J Exp Med* (1998) 188:1485–92. doi: 10.1084/jem.188.8.1485

31. Kuo PT, Zeng Z, Salim N, Mattarollo S, Wells JW, Leggatt GR. The role of CXCR3 and its chemokine ligands in skin disease and cancer. *Front Med (Lausanne)* (2018) 5:271. doi: 10.3389/fmed.2018.00271

32. Placek K, Coffre M, Maiella S, Bianchi E, Rogge L. Genetic and epigenetic networks controlling T helper 1 cell differentiation. *Immunology* (2009) 127:155–62. doi: 10.1111/j.1365-2567.2009.03059.x

33. Cano-Gamez E, Soskic B, Roumeliotis TI, So E, Smyth DJ, Baldrighi M, et al. Single-cell transcriptomics identifies an effectorness gradient shaping the response of CD4 + T cells to cytokines. *Nat Commun* (2020) 11:1801. doi: 10.1038/s41467-020-15543-y

34. Ding X, Chang Y, Wang S, Yan D, Yao J, Zhu G. Transcriptomic analysis of the effect of GAT-2 deficiency on differentiation of mice naïve T cells into Th1 cells *In vitro*. *Front Immunol* (2021) 12:667136. doi: 10.3389/fimmu.2021.667136

35. Rothe K, Bismarck D, Büttner M, Alber G, von Buttlar H. Canine peripheral blood CD4+CD8+ double-positive tcell subpopulations exhibit distinct tcell phenotypes and effector functions. *Vet Immunol Immunopathol* (2017) 185:48–56. doi: 10.1016/j.vetimm.2017.01.005

36. Evans-Marin HL, Cao AT, Yao S, Chen F, He C, Liu H, et al. Unexpected regulatory role of CCR9 in regulatory T cell development. *PloS One* (2015) 10:e0134100. doi: 10.1371/journal.pone.0134100

37. Rudra D, deRoos P, Chaudhry A, Niec RE, Arvey A, Samstein RM, et al. Transcription factor Foxp3 and its protein partners form a complex regulatory network. *Nat Immunol* (2012) 13:1010–9. doi: 10.1038/ni.2402

38. Wohlfert EA, Grainger JR, Bouladoux N, Konkel JE, Oldenhove G, Ribeiro CH, et al. GATA3 controls Foxp3$^+$ regulatory T cell fate during inflammation in mice. *J Clin Invest* (2011) 121:4503–15. doi: 10.1172/JCI57456

39. Wang Y, Su MA, Wan YY. An essential role of the transcription factor GATA-3 for the function of regulatory T cells. *Immunity* (2011) 35:337–48. doi: 10.1016/j.immuni.2011.08.012

40. Hsu DK, Chen H-Y, Liu F-T. Galectin-3 regulates T-cell functions. *Immunol Rev* (2009) 230:114–27. doi: 10.1111/j.1600-065X.2009.00798.x

41. Chattopadhyay PK, Yu J, Roederer M. A live-cell assay to detect antigen-specific CD4+ T cells with diverse cytokine profiles. *Nat Med* (2005) 11:1113–7. doi: 10.1038/nm1293

42. Bacher P, Scheffold A. Flow-cytometric analysis of rare antigen-specific T cells. *Cytometry A* (2013) 83:692–701. doi: 10.1002/cyto.a.22317

43. Ebner F, Schwiertz P, Steinfelder S, Pieper R, Zentek J, Schütze N, et al. Pathogen-reactive T helper cell analysis in the pig. *Front Immunol* (2017) 8:565. doi: 10.3389/fimmu.2017.00565

44. Schnabel CL, Fletemeyer B, Lübke S, Marti E, Wagner B, Alber G. CD154 expression indicates T cell activation following tetanus toxoid vaccination of horses. *Front Immunol* (2022) 13:805026. doi: 10.3389/fimmu.2022.805026

45. Prajapati K, Perez C, Rojas LB, Burke B, Guevara-Patino JA. Functions of NKG2D in CD8+ T cells: an opportunity for immunotherapy. *Cell Mol Immunol* (2018) 15:470–9. doi: 10.1038/cmi.2017.161

46. van Aalderen MC, Remmerswaal EB, ten Berge IJ, van Lier RA. Blood and beyond: properties of circulating and tissue-resident human virus-specific αβ CD8(+) T cells. *Eur J Immunol* (2014) 44:934–44. doi: 10.1002/eji.201344269

47. Garner LC, Klenerman P, Provine NM. Insights into mucosal-associated invariant T cell biology from studies of invariant natural killer T cells. *Front Immunol* (2018) 9:1478. doi: 10.3389/fimmu.2018.01478

48. Hayday AC. Gammadelta cells: A right time and a right place for a conserved third way of protection. *Annu Rev Immunol* (2000) 18:975–1026. doi: 10.1146/annurev.immunol.18.1.975

49. Kruse PH, Matta J, Ugolini S, Vivier E. Natural cytotoxicity receptors and their ligands. *Immunol Cell Biol* (2014) 92:221–9. doi: 10.1038/icb.2013.98

50. Legoux F, Salou M, Lantz O. MAIT cell development and functions: the microbial connection. *Immunity* (2020) 53:710–23. doi: 10.1016/j.immuni.2020.09.009

51. Koay H-F, Godfrey DI, Pellicci DG. Development of mucosal-associated invariant T cells. *Immunol Cell Biol* (2018) 96:598–606. doi: 10.1111/imcb.12039

52. Erkers T, Xie BJ, Kenyon LJ, Smith B, Rieck M, Jensen KP, et al. High-parametric evaluation of human invariant natural killer T cells to delineate heterogeneity in allo- and autoimmunity. *Blood* (2020) 135:814–25. doi: 10.1182/blood.2019001903

53. Khan O, Giles JR, McDonald S, Manne S, Ngiow SF, Patel KP, et al. TOX transcriptionally and epigenetically programs CD8+ T cell exhaustion. *Nature* (2019) 571:211–8. doi: 10.1038/s41586-019-1325-x

54. Alfei F, Kanev K, Hofmann M, Wu M, Ghoneim HE, Roelli P, et al. TOX reinforces the phenotype and longevity of exhausted T cells in chronic viral infection. *Nature* (2019) 571:265–9. doi: 10.1038/s41586-019-1326-9

55. Yao C, Sun H-W, Lacey NE, Ji Y, Moseman EA, Shih H-Y, et al. Single-cell RNA-seq reveals TOX as a key regulator of CD8+ T cell persistence in chronic infection. *Nat Immunol* (2019) 20:890–901. doi: 10.1038/s41590-019-0403-4

56. Schuldt NJ, Binstadt BA. Dual TCR T cells: Identity crisis or multitaskers? *J Immunol* (2019) 202:637–44. doi: 10.4049/jimmunol.1800904

57. Gutierrez-Arcelus M, Teslovich N, Mola AR, Polidoro RB, Nathan A, Kim H, et al. Lymphocyte innateness defined by transcriptional states reflects a balance between proliferation and effector functions. *Nat Commun* (2019) 10:687. doi: 10.1038/s41467-019-08604-4

58. Brigl M, Bry L, Kent SC, Gumperz JE, Brenner MB. Mechanism of CD1d-restricted natural killer T cell activation during microbial infection. *Nat Immunol* (2003) 4:1230–7. doi: 10.1038/ni1002

59. Cesano A, Visonneau S, Clark SC, Santoli D. Cellular and molecular mechanisms of activation of MHC nonrestricted cytotoxic cells by IL-12. *J Immunol* (1993) 151:2943–57. doi: 10.4049/jimmunol.151.6.2943

60. Ussher JE, Bilton M, Attwod E, Shadwell J, Richardson R, de LC, et al. CD161++ CD8+ T cells, including the MAIT cell subset, are specifically activated by IL-12+IL-18 in a TCR-independent manner. *Eur J Immunol* (2014) 44:195–203. doi: 10.1002/eji.201343509

61. Chou C, Zhang X, Krishna C, Nixon BG, Dadi S, Capistrano KJ, et al. Programme of self-reactive innate-like T cell-mediated cancer immunity. *Nature* (2022) 605:139–45. doi: 10.1038/s41586-022-04632-1

62. Correia MP, Stojanovic A, Bauer K, Juraeva D, Tykocinski L-O, Lorenz H-M, et al. Distinct human circulating NKp30+FcεRIγ+CD8+ T cell population exhibiting high natural killer-like antitumor potential. *Proc Natl Acad Sci USA* (2018) 115:E5980–9. doi: 10.1073/pnas.1720564115

63. Liang C, Huang S, Zhao Y, Chen S, Li Y. TOX as a potential target for immunotherapy in lymphocytic malignancies. *biomark Res* (2021) 9:20. doi: 10.1186/s40364-021-00275-y

64. Boudinot P, Mondot S, Jouneau L, Teyton L, Lefranc M-P, Lantz O. Restricting nonclassical MHC genes coevolve with TRAV genes used by innate-like T cells in mammals. *Proc Natl Acad Sci USA* (2016) 113:E2983–92. doi: 10.1073/pnas.1600674113

65. Yasuda N, Masuda K, Tsukui T, Teng A, Ishii Y. Identification of canine natural CD3-positive T cells expressing an invariant T-cell receptor alpha chain. *Vet Immunol Immunopathol* (2009) 132:224–31. doi: 10.1016/j.vetimm.2009.08.002

66. Schjaerff M, Keller SM, Affolter VK, Kristensen AT, Moore PF. Cellular endocytic compartment localization of expressed canine CD1 molecules. *Vet Immunol Immunopathol* (2016) 182:11–21. doi: 10.1016/j.vetimm.2016.08.012

67. van Looringh Beeck FA, Leegwater PA, Herrmann T, Broere F, Rutten VP, Willemse T, et al. Tandem repeats modify the structure of the canine CD1D gene. *Anim Genet* (2013) 44:352–5. doi: 10.1111/age.12002

68. Alexandre-Pires G, de Brito MT, Algueró C, Martins C, Rodrigues OR, Da Fonseca IP, et al. Canine leishmaniasis. immunophenotypic profile of leukocytes in different compartments of symptomatic, asymptomatic and treated dogs. *Vet Immunol Immunopathol* (2010) 137:275–83. doi: 10.1016/j.vetimm.2010.06.007

69. Schütze N, Raue R, Büttner M, Alber G. Inactivated parapoxvirus ovis activates canine blood phagocytes and T lymphocytes. *Vet Microbiol* (2009) 137:260–7. doi: 10.1016/j.vetmic.2009.01.035

70. Otani I, Ohta K, Ishikawa A, Yamada T, Ishinazaka T, Ohtaki T, et al. Flow cytometric analysis of canine umbilical cord blood lymphocytes. *J Vet Med Sci* (2008) 70:285–7. doi: 10.1292/jvms.70.285